AIMS Materials Science, 11(2): 243–255.
DOI: 10.3934/matersci.2024014
Received: 09 January 2024
Revised: 10 February 2024
Accepted: 21 February 2024
Published: 28 February 2024

http://www.aimspress.com/journal/Materials

Research article

Effect of sintering temperatures on the physical, structural properties and microstructure of mullite-based ceramics

Mohamed Lokman Jalaluddin[1], Umar Al-Amani Azlan[1,*], Mohd Warikh Abd Rashid[1] and Norfauzi Tamin[2]

[1] Faculty of Technology and Industrial and Manufacturing Engineering, Universiti Teknikal Malaysia Melaka, Malaysia
[2] Faculty of Technical and Vocational Education, Universiti Tun Hussien Onn Malaysia, Parit Raja, Johor, Malaysia

*** Correspondence:** Email: umar@utem.edu.my; Tel: +6-06-270-4020; Fax: +6-06-270-1065.

Abstract: This study explored the impact of sintering temperature variations on the synthesis and characteristics of mullite ceramics derived from a composite blend of kaolinite clay, silica (silicon dioxide), and feldspar. Sintering temperatures ranging from 1100 to 1200 °C were systematically examined to analyze alterations in shrinkage, density, microstructure, elemental composition, and phase formation. The study revealed that an increase in sintering temperature led to decreased shrinkage due to improved particle packing and reduced porosity. Ceramic density showed a direct relation with sintering temperature, reaching the optimal density at 1175 °C and indicating efficient particle packing and compaction. Analysis through field emission scanning electron microscopy (FESEM) provided insights into microstructural changes, including alterations in grain morphology, porosity, and connectivity. Energy dispersive X-ray spectroscopy (EDS) clarified element distribution within the microstructure, offering valuable information on compositional variations. X-ray diffraction (XRD) examinations unveiled temperature-dependent phase transformations, which confirmed the successful formation of mullite during the sintering process. A sintering temperature of 1175 °C yielded the optimal ceramic quality and cost-effectiveness for high-temperature heating processes.

Keywords: sintering temperature; mullite ceramic; physical; structural; microstructure

1. Introduction

The present need for interior spaces' environmental comfort necessitates the utilization of building air conditioning systems to regulate climate conditions and uphold relatively stable temperatures. To decrease the usage of energy, it is necessary to limit the inflow of outside air, the thermal properties of which are frequently distinct from those intended. This suggests the need for the creation of structures that are more hermetically sealed and possess superior thermal insulation. However, this approach can potentially result in detrimental moisture issues and diminished air quality. The expansion of energy demand for cooling is expected to become prevalent in buildings by 2050, with an average rise of more than 75%. Furthermore, the rise in power usage is followed by an increase in emissions of carbon dioxide (CO_2) [1,2]. Therefore, it is not surprising that the scientific community has demonstrated a significant interest in developing materials that have potential to reduce or finally eliminate the need for air conditioning. One of the proposed solutions entails developing a porous ceramic material with an intrinsic ability to control humidity and guarantee that indoor humidity levels remain within the human comfort zone, which normally ranges between 40% and 70% [3].

Ceramic tiles have adorned our living spaces for millennia, defying fads and trends to remain a symbol of utilitarian endurance and aesthetic appeal. A transforming process known as sintering is at the core of every ceramic tile journey from raw clay to works of design for buildings and interiors [4]. Sintering is a key stage in the production of ceramic tiles. It is sometimes described as an alchemical process of transforming earthy ingredients to strong and sturdy works of art. It is a process in which an apparently common composition of clay and minerals is exposed to the tremendous heat of transformation, resulting in a product of utility as well as aesthetics [5,6]. One of the most important technological processes in conventional ceramic manufacture is sintering. During this stage, the shape established in the formation phase is consolidated [7]. The interaction of various raw materials when exposed to heat often determines the type of product and its technical attributes, such as firing temperature and duration of the firing cycle. Therefore, understanding sensitivity to alterations of a ceramic body in the firing cycle is significant [8]. The sintering temperature influences both density and porosity of ceramic tiles. As temperature rises during sintering, clay particles in the raw material mix, soften, and partially melt. This softening process allows chemical linkages to form between neighbouring particles, resulting in increased density. Increased sintering temperatures often result in decreased porosity, which improves the resistance of tile to moisture infiltration and discoloration [9,10].

Ceramics based on mullite have garnered considerable attention because of their impressive characteristics, including outstanding thermal and electrical insulation, remarkable thermal stability, excellent resistance to thermal shock, a low coefficient of thermal expansion, superb resistance to creep, and high tolerance to damage and corrosion [11–14]. The combination of these qualities renders ceramics based on mullite a favoured material for an array of technical uses, such as premium-grade refractories, molten metal filters, substrates for electronics, carriers for catalysts, packaging for microelectronics, and materials for structural purposes [15–17]. Mullite is uncommon in nature due to the limited circumstances under which it forms. Mullite ceramics are typically manufactured on an industrial scale [18,19]. This mullite is used as a base material for low thermal conductivity in ceramic tiles. The research problem revolves around understanding how sintering temperature impacts the properties and characteristics of ceramic particularly for mullite based materials. This study provides insights into the physical and structural properties, as well as microstructure, for determining optimal

sintering parameters that achieve desired material characteristics and performance in ceramics. It considers factors such as cost-effectiveness and energy efficiency.

Based on the previous problems, it is important to determine the optimal sintering temperature conditions for achieving specific material properties in ceramics. This goal is to precisely identify the sintering temperature range that best matches with intended material attributes in ceramics. It will determine the specific temperature at which ceramics display the necessary qualities, such as a defined amount of density and phase composition, by systematically adjusting and testing the sintering temperatures. This technique guarantees that ceramic materials may be designed to satisfy the precise requirements of various applications, ranging from sophisticated structural components to high-temperature insulators, maximizing their usability and performance across a wide range of industrial and technical sectors. Furthermore, it analyses the influence of varying sintering temperatures on the microstructural properties of ceramic materials. This goal entails conducting a thorough examination of how changes in sintering temperature affect the microstructure of ceramic materials. By subjecting ceramics to a range of sintering temperatures and carefully examining their microstructural properties, including grain size, porosity, and phase distribution, we aimed to discern patterns and correlations. This aim yields crucial insights into the fundamental associations between sintering temperature and internal composition of ceramics, thus guiding the optimization of sintering processes tailored for specific applications. In addition, it helps us to understand the phase transformations and crystalline structure changes in ceramics due to sintering temperature variations. This goal is to delve into the complex interplay between changes in sintering temperature and the alterations in ceramic phases and crystalline structures. This study wants to uncover the specific mechanisms and patterns behind these changes by submitting ceramics to varied sintering temperatures and conducting comprehensive analyses. Understanding how temperature affects phase transitions and crystal configurations is critical for customising ceramic materials for specific uses.

2. Materials and methods

2.1. Materials

Ceramic samples were created by utilizing a blend of clay (kaolinite) (Anji Runxing New Materials Co., Ltd.), silica (silicon dioxide) (CABOT Corporation), and feldspar (Multifilla^{TM}), resulting in a mixture which included microcline. The mixture had a chemical formula of $Al_2Si_2O_5(OH)_4 + SiO_2 + KAlSi_3O_8$. The combination had a total weight of 100 g, and the individual component weights can be determined through the chemical equation. Furthermore, the amounts of clay, silica, and feldspar were 43.28, 10.07, and 46.65 g, respectively.

2.2. Sample preparation

To manufacture ceramic structural samples, both disk and bar shapes were employed. The bar-shaped samples had average dimensions of 75 mm in length, 10 mm in width, and 5 mm in height, whereas the disc-shaped sample had a diameter of 13 mm and 4 mm of thickness. By using a total of 100 g of material, five distinct ceramic combinations were created for temperatures of 1100, 1125, 1150, 1175, and 1200 °C. The clay and feldspar components were initially in solid form and were crushed to the desired consistency by using a mortar and pestle, whereas silica was in powdered form. These raw

materials were mixed by using ball milling to get a constant size distribution. Three sintered ceramic samples were produced from each mixture, resulting in a grand total of 30 sintered samples. In this research, sintering temperatures were determined based on a single temperature ramp-up curve. The temperature was raised incrementally, with a 5 °C/min, until the target sintering temperature was attained. Upon achieving this, the material was permitted to naturally cool to the typical room temperature range of approximately 25–28 °C. Before the powder was consolidated, it was warmed, which caused it to oxidize and prevented it from breaking free from the framework. As previously stated, ceramic samples were created in the shapes of bars and discs. The preference for the bar shape stems was due to its ability to evenly compress the powder through uniaxial loading, with dimensions averaging 75 mm in length, 10 mm in width, and 5 mm in height. In contrast to the square tile configuration, this shape necessitates a minimal quantity of material. In this technique, an SM100 universal testing machine was utilized to create ceramic structures. At first, both disc and bar molds were filled with ceramic powder. Following this step, the mold was positioned within the universal testing machine and subjected to 20 MPa of pressure for a duration of 60 s. With enough effort, this process concluded in the production of bars or disc-shaped structures. These discoveries emphasized the critical role of dry pressing in determining the applied force on the sample.

2.3. Material characterization

To determine the shrinkage of a ceramic sample, its dimensions before and after firing were compared. Shrinkage is often stated as a percentage of the original size. Before heating the ceramic sample, its dimensions were measured by using a digital vernier caliper. Diameter of the ceramic sample was recorded. The ceramic sample was fired by using the approved firing schedule. The degree of shrinkage can be affected by the fire temperature and time. The ceramic sample temperature was allowed to drop to room temperature after firing. The cooling period was crucial because the ceramic may continue to change its size during this time. After the ceramic sample had cooled, its dimensions were again measured using the same digital vernier caliper. The diameter of the ceramic sample was measured after firing. To get the percentage of shrinkage for each dimension, the following formula was applied as in Eq 1.

$$Shrinkage\ percentage = \left(\frac{initial\ dimension - final\ dimension}{initial\ dimension}\right) \times 100\% \quad (1)$$

According to Archimedes' principle, the upward force acting on a submerged object is equivalent to the weight of the fluid that the object displaces. The Archimedes buoyancy method was employed for density determination. Dry mass was represented by *Wa*, mass suspended in water was represented by *Wb*, and saturated mass was represented by *Wc*. To calculate the density formula, the mass (*Wa*) of the sample was precisely measured by using an A&D FZ-300i EC precision balance after it was heated. The sample was subsequently immersed in distilled water briefly, and measurements for *Wb* and *Wc* were taken by utilizing the same scale. The acquired data was examined to derive the formula for density. The density of each sample was subsequently computed by applying Archimedes' fundamental formula as shown in Eq 2.

$$D = \frac{Wa}{Wc - Wb} \quad (2)$$

Field emission scanning electron microscopy (FESEM) is an advanced technique employed to image material microstructures, typically conducted within a vacuum environment. This arises from the potential for gas molecules to disrupt the electron beam and the essential secondary and backscattered electrons needed for imaging. Microstructural images of the samples in this study were captured by using a JEOL JSM-6010PLUS/LV instrument for analysis. The top surface samples were examined in this study, which required multiple preparation stages, such as grinding, polishing, and thermal etching, ahead of FESEM analysis. Grinding of each sample was performed by using abrasive papers with grit sizes of 1000, 1500, and 2000. To guarantee that the surface of sample was free of scratches, the grinding procedure was carried out according to the grain size of the abrasive paper. Each sample underwent a brief grinding process, followed by polishing using a micro pad and 0.05 μm Al_2O_3. Following the completion of grinding and polishing, the samples were rapidly oven dried at 60 ℃ for less than 1 min. After drying, the thermal etching process was applied to all samples by immersing them in a 1100 ℃ environment for 1 min. Prior to scanning, it was essential to ensure that the sample was both dried and thoroughly cleaned. An adhesive tab was applied to the aluminium stub to mount the sample. The vacuum chamber was vented, allowing for the removal of air. The sample was subsequently positioned in the sample holder, and the chamber door was sealed. The vacuum pump operated until it achieved the highest vacuum level. When this was completed, the sample was ready for testing. Lastly, sintered samples subjected to varying sintering temperatures were analysed using an X-ray diffraction (XRD) instrument, namely, the PANalytical X'Pert PRO. The XRD analysis was employed for identifying the crystalline phases within a material, thereby providing insight into its chemical composition.

3. Results and discussion

3.1. Analysis of shrinkage and bulk density of sintering ceramic sample

Among the limited observable alterations in samples subjected to various temperatures, there were differences in dimensions, including diameter and shape. The initial diameter of a sample before burning in the furnace was 12.92 mm. An increase in the temperature utilized for sample combustion resulted in shrinkage. As per the information provided in Table 1, the average diameter of samples subjected to a temperature of 1100 ℃ was 12.20 mm, while at 1125 ℃ it was 11.99 mm, at 1150 ℃ it was 11.91 mm, at 1175 ℃ it was 11.99 mm, and at 1200 ℃ it was 12.04 mm. Based on Figure 1, the percentage of shrinkage was highest at 1150 ℃. At 1100 and 1125 ℃, the percentage of shrinkage was lower, and the ceramic samples' surfaces still appeared powdery. Meanwhile, at 1200 ℃, the ceramic samples appeared glassy, stuck to the crucible after firing in the furnace, and were no longer disc shaped. The percentage of shrinkage at 1175 ℃ (7.22%) was lower than that at 1150 ℃ (7.82%), and the sample was disc shaped and did not stick to the crucible. Sample shrinkage occurs for several reasons. Initially, the reduction in sample size was attributed to the evaporation of water during densification. Clay soil typically holds about 20% water and 9% organic matter. Despite the clay being dried before entering the kiln, it retained a small amount of moisture [20].

Table 1. Shrinkage of the ceramic samples after different sintering temperatures.

Temperature (°C)	Sample 1 (mm)	Sample 2 (mm)	Sample 3 (mm)	Average (mm)	Percentage of shrinkage (%)
1100	12.20	12.22	12.17	12.20	5.57
1125	11.95	12.01	12.00	11.99	7.20
1150	11.88	11.97	11.88	11.91	7.82
1175	11.95	12.02	11.99	11.99	7.20
1200	12.04	12.04	12.04	12.04	6.81

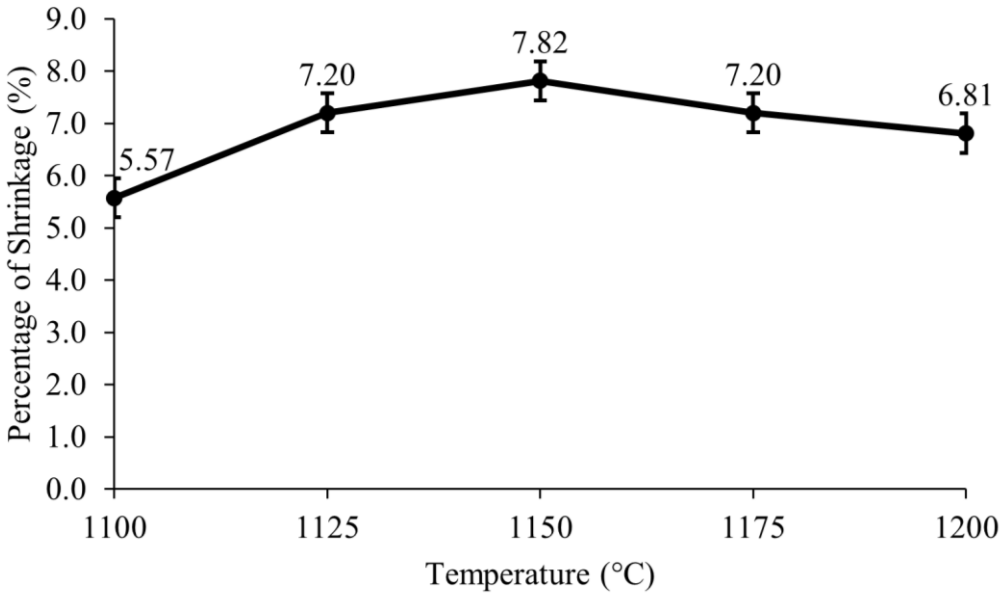

Figure 1. Shrinkage variation with temperature in ceramic samples.

Table 2 and Figure 2 present the variation in bulk density for ceramic samples at different sintering temperatures, including 1100, 1125, 1150, 1175, and 1200 °C. The bulk density values showed a rise as the sintering temperature increased from 1100 to 1175 °C. Consequently, incremental sintering through higher-temperature firing resulted in a more compact ceramic structure, accompanied by the development of a glassy phase that filled the pores [21]. The rise in bulk density with fire might be due to the creation of a glassy phase with a more prominent liquid phase and lower porosity [22]. The peak bulk density, which reached 2.32 g/cm^3 with a relative density percentage of 99.80%, was attained at the sintering temperature of 1175 °C. In ceramic materials, particle size and distribution can influence shrinkage and density. Non-uniform particle packing can cause changes in compaction and, therefore, in shrinkage and density [23]. At the sintering temperature of 1175 °C, the density was the highest due to particle distribution in the sample, even though the percentage of shrinkage was lower as compared to the sintering temperature of 1150 °C.

Table 2. Density measurements at different sintering temperatures.

Temperature (°C)	Sample	*Wa* (g)	*Wb* (g)	*Wc* (g)	Density of sample (g/cm^3)	Average density of sample (g/cm^3)	Density of the reference substance (g/cm^3)	Average density of the reference substance (g/cm^3)	Relative density (%)
1100	1	0.98	0.56	0.99	2.28		2.26		
	2	0.96	0.54	1.00	2.09	2.18	2.31	2.29	94.34
1125	1	0.95	0.55	0.96	2.32		2.36		
	2	0.95	0.55	0.97	2.26	2.29	2.33	2.34	97.61
1150	1	0.96	0.56	0.97	2.34		2.39		
	2	0.95	0.55	0.97	2.26	2.30	2.37	2.38	96.99
1175	1	0.94	0.53	0.94	2.29		2.33		
	2	0.94	0.55	0.95	2.35	2.32	2.33	2.33	99.80
1200	1	0.94	0.52	0.94	2.24		2.29		
	2	0.95	0.54	0.96	2.26	2.25	2.28	2.28	98.51

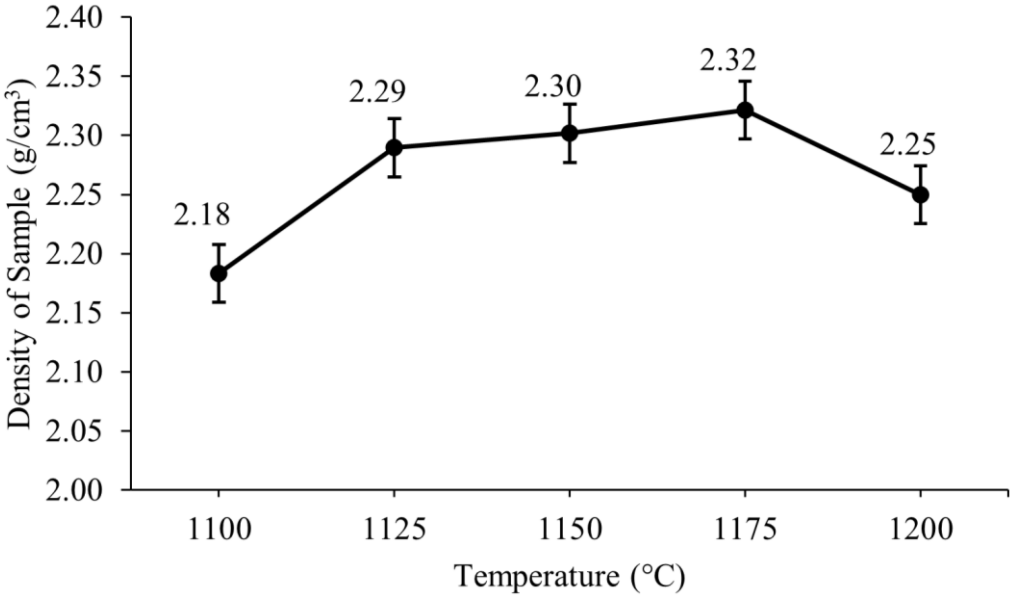

Figure 2. Relationship between sintering temperature and density.

3.2. Analysis of crystal structure and phase composition using XRD

Figure 3 depicts the crystal structure and phase composition of ceramic sintered at various temperatures. Silicon dioxide (SiO_2) and mullite ($3Al_2O_3{\cdot}2SiO_2$) were identified in all samples. The dried green body of ceramic with kaolinite ($2Al_2Si_2O_5(OH)_4$) phase was converted into quartz (SiO_2) and mullite at high temperatures of over 1000 °C and low-pressure conditions. Existence of the mullite phase played a crucial role in achieving ceramics that exhibited strong chemical and thermal stability, as well as excellent resistance to creep [24]. Furthermore, the inclusion of feldspar in the ceramic composition enhanced its thermal stability, leading to increased bond strength between the compounds, particularly when the sintering temperature surpassed 1140 °C [25].

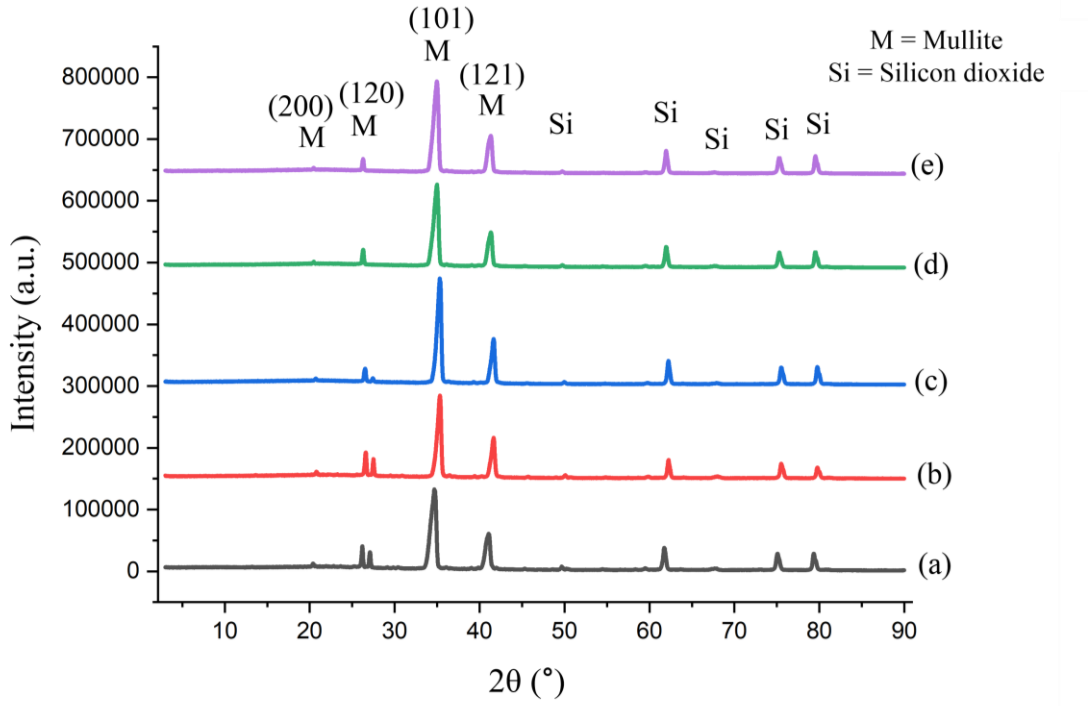

Figure 3. XRD analysis was performed on mullite ceramics following sintering at distinct temperatures: (a) 1100, (b) 1125, (c) 1150, (d) 1175, and (e) 1200 °C.

Figure 3 displays the XRD patterns of the ceramic samples sintered at different temperatures: 1100, 1125, 1150, 1175, and 1200 °C. Several diffraction peaks were visible in each pattern, indicating the presence of crystalline phases. This aligned with the observation that the full conversion of aluminosilicate into mullite takes place at temperatures which exceed 1400 °C, giving rise to the formation of the mullite phase [26]. All the diffraction peaks corresponding to mullite in the XRD pattern exhibited a close match with the PDF card number 01-070-5689 data for mullite, which possesses an orthorhombic crystal structure in the *Pbam* space group. The XRD pattern of the tested material is shown in Figure 3, with the most prominent peaks for mullite located at 2θ angles of approximately 27.32, 33.18 and 40.90°. These peaks corresponded to the (120), (101) and (121) planes, respectively. Further, the most prominent peaks for silicon dioxide were located at 2θ angles of approximately 49.99, 62.55, and 80.92°. These peaks corresponded to the (012), (022), and (032) planes, respectively. The XRD analysis for the mullite phase revealed that the examined material possessed an orthorhombic crystal structure with lattice parameters a = 7.52 Å and c = 2.89 Å, providing valuable insight into the atomic organization of the material. The prominence of (101) and (121) peaks strongly implied a preferential orientation of the material along these specific crystallographic planes. Moreover, the silicon dioxide phase revealed that the examined material possessed a monoclinic crystal structure with lattice parameters a = 6.674 Å and c = 4.625 Å, providing valuable insight into the atomic organization of the material.

Furthermore, the XRD examination showed that no new phases emerged at higher sintering temperatures, indicating that the orthorhombic and monoclinic phases were stable within the temperature range examined. The increasing intensity of these peaks at higher sintering temperatures could be attributed to improved crystallite formation and decreased imperfections in the crystal lattice of the material. As a result, mechanical characteristics and structural integrity increased [27]. In

summary, XRD research indicated that sintering temperature had a substantial impact on the crystalline structure of ceramic materials [28]. Higher sintering temperatures promoted crystallinity and the appearance of orthorhombic and monoclinic phases, which were linked with improved material characteristics. This discovery has implications for improving the sintering process in ceramic production to attain necessary material properties.

3.3. Morphological characteristics through elemental analysis of the surface

Figure 4 illustrates how the microstructure of the samples is influenced by variations in sintering temperature by FESEM. When subjected to low sintering temperatures, specifically at 1100 and 1125 °C, the ceramic microstructure presented a comparatively open and porous arrangement. With a rise in sintering temperature to 1150 and 1175 °C, the ceramic microstructure underwent a transformation toward higher density, featuring fewer pores and a greater degree of interconnection among the grains. As shown in Table 2, the relative density of 1175 °C was the highest, at 99.80%. Therefore, the interconnection among the grains had strong bonding. When sintered at an elevated temperature of 1200 °C, the ceramic underwent considerable grain expansion, resulting in a finer microstructure characterized by minimal porosity, and the relative density was 98.51%. According to the relative density, the sintering temperature of 1200 °C had the lowest density. Therefore, the microstructures of the ceramics were influenced by the sintering temperature. At lower temperatures, there was inadequate energy available for promoting effective grain bonding, which resulted in an open and porous structure. However, with an increase in sintering temperature, ceramic particles diffuse and sinter more efficiently, leading to a denser microstructure [29,30]. This could have a substantial impact on the mechanical and thermal properties of the material [31].

Energy dispersive X-ray spectroscopy (EDS) was employed to determine the elemental compositions of the prevailing phases. Table 3 shows the EDS findings for samples subjected to firing temperatures of 1100, 1125, 1150, 1175, and 1200 °C. The EDS findings indicated the presence of Al, Si, and O in the samples, signifying that the crystals corresponded to mullite. The formation of mullite crystals was less apparent for the 1100 and 1125 °C sintering temperatures, while a more significant quantity of mullite grain was generated at the 1200 °C sintering temperature. At 1175 °C, the concentration of mullite was at its peak, and the grain growth was most favourable. This suggested that elevated sintering temperatures facilitated the creation and advancement of mullite. The Al content in the sample at 1175 °C was greater than that at 1150 °C, as shown in Table 3, providing additional support for the idea that kaolinite $Al_2Si_2O_5(OH)_4$ contributed to the formation of mullite. It was also confirmed by EDS that the mullite is present in the compound.

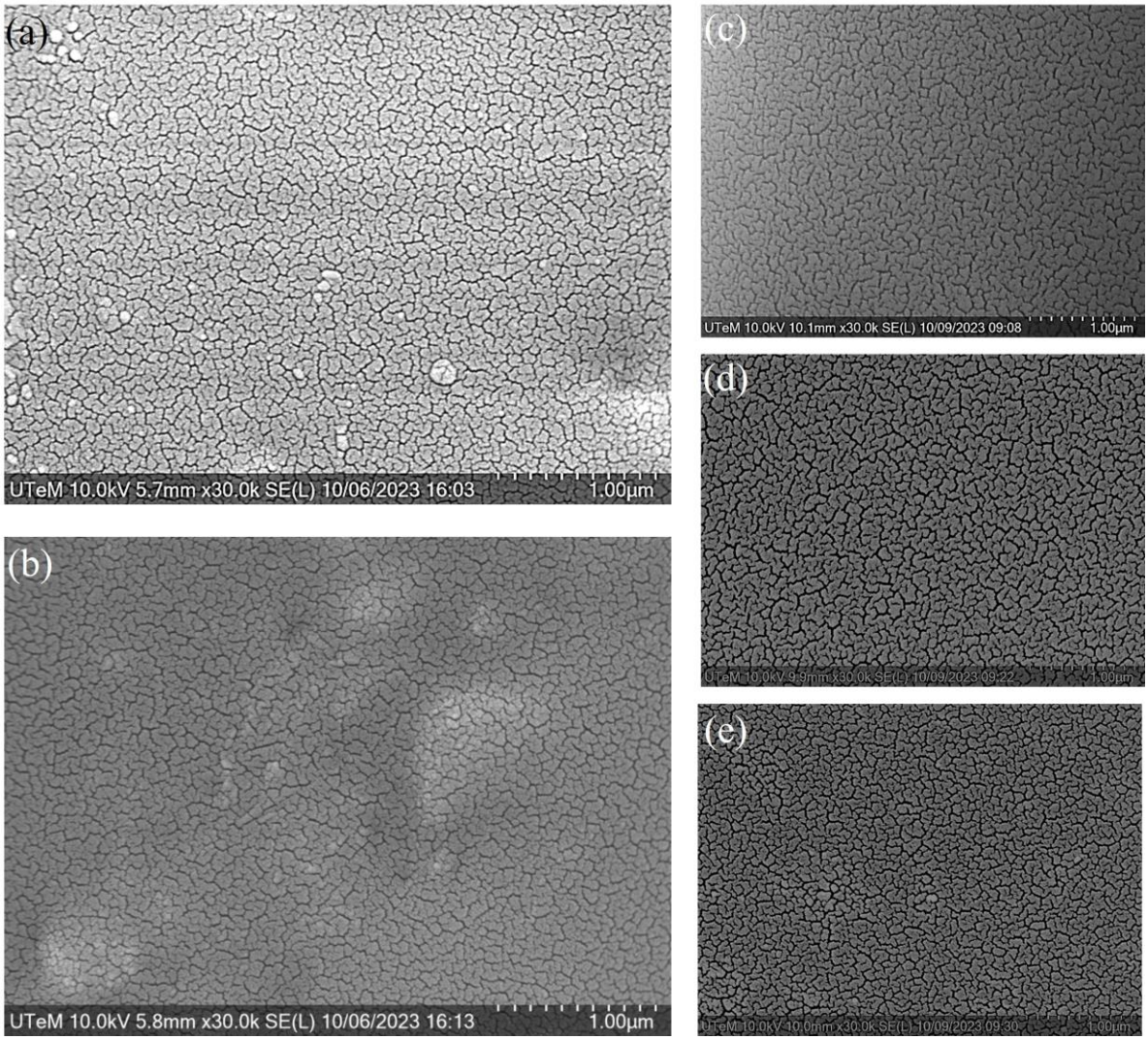

Figure 4. FESEM images were obtained for ceramic samples sintered at different temperatures: (a) 1100, (b) 1125, (c) 1150, (d) 1175, and (e) 1200 °C.

Table 3. The element results of EDS for different sintering temperatures.

Temperature (°C)	O (%)	Al (%)	Si (%)	K (%)
1100	43.0	8.7	22.5	4.9
1125	38.1	8.7	24.9	4.3
1150	43.6	6.7	24.6	3.3
1175	38.0	8.1	23.8	5.0
1200	41.9	8.9	23.4	4.8

4. Conclusions

In conclusion, the appropriate sintering temperature for mullite ceramics has been successfully determined by using clay (kaolinite), silica (silicon dioxide), and feldspar. The characteristics of the final ceramic product were observed to be significantly influenced by both qualitative and quantitative composition of the formulated powder (clay, feldspar, silica) as well as sintering temperature. In this

investigation, the sample sintered at 1175 °C proved to be the most favorable, exhibiting the highest density, effective particle packing, and minimal porosity. The density findings were supported by the microstructural investigation, which showed a definite change in the ceramic microstructure with changing sintering temperatures. At greater temperatures, grains became more tightly packed, and pores shrank, resulting in increased material density. The observed growth in grain size at higher sintering temperatures suggested intensified grain growth. Furthermore, XRD analysis revealed potential phase transformations, underscoring the importance of meticulous control over sintering conditions. This investigation underscored the significance of selecting the sintering temperature according to the intended application. In the case of structured ceramics, opting for higher sintering temperatures may be preferable to achieve optimal density and strength. Conversely, lower temperatures might be suitable for applications, whereby controlled porosity was beneficial. Potential areas for further research could involve examining the impact of residence time on peak temperature, studying the influences of various atmospheres during the sintering process, and gaining insights into the long-term stability of microstructures and optimized properties. To conclude, this study provides valuable insight into the intricate connection between sintering temperature and ceramic properties. The knowledge acquired can serve as a guide for manufacturing processes and play a pivotal role in creating ceramics with customized properties for a wide range of industrial applications.

Use of AI tools declaration

The authors declare they have not used artificial intelligence (AI) tools in the creation of this article.

Acknowledgments

The authors extend their appreciation to the Skim Zamalah Universiti Teknikal Malaysia Melaka (UTeM), as well as to UTeM for funding this research work through project number PJP/2020/FTKMP/TD/S01727.

Conflict of interest

The authors declare that they have no conflict of interest.

References

1. Pacheco R, Ordóñez J, Martínez G (2012) Energy efficient design of building: A review. *Renew Sust Energ Rev* 16: 3559–3573. https://doi.org/10.1016/j.rser.2012.03.045
2. Mirrahimi S, Mohamed MF, Haw LC, et al. (2016) The effect of building envelope on the thermal comfort and energy saving for high-rise buildings in hot–humid climate. *Renew Sust Energ Rev* 53: 1508–1519.https://doi.org/10.1016/j.rser.2015.09.055
3. Tian W, Shui A, Ke S, et al. (2019) Low-temperature preparation of humidity self-regulating porous ceramics with high strength performance. *Mater Lett* 243: 128–131. https://doi.org/10.1016/j.matlet.2019.02.019

4. Boschi G, Bonvicini G, Masi G, et al. (2023) Recycling insight into the ceramic tile manufacturing industry. *Open Ceram* 16: 100471. https://doi.org/10.1016/j.oceram.2023.100471
5. Sokolar R, Nguyen M (2022) Sintering of anorthite ceramic body based on interstratified illite-smectite clay. *Ceram Int* 48: 31783–31789. https://doi.org/10.1016/j.ceramint.2022.07.105
6. Castellano J, Sanz V, Cañas E, et al. (2022) Effect of firing temperature on humidity self-regulation functionality in a ceramic tile composition. *J Eur Ceram Soc* 42: 6236–6243. https://doi.org/10.1016/j.jeurceramsoc.2022.05.058
7. Azevedo ARG, França BR, Alexandre J, et al. (2018) Influence of sintering temperature of a ceramic substrate in mortar adhesion for civil construction. *J Build Eng* 19: 342–348. https://doi.org/10.1016/j.jobe.2018.05.026
8. Pinto MF, Sousa SJG, Holanda JNF (2005) Effect of the firing cycle on the technological properties of a red ceramic mass for porous coating. *Ceramica* 51: 225–229. https://doi.org/10.1016/j.matpr.2024.01.022
9. Şan O, Koç M, Cengizler H (2019) Production of porous ceramic from clinoptilolite incorporating aluminum powder. *Ceram Int* 45: 24037–24043. https://doi.org/10.1016/j.ceramint.2019.08.108
10. Li B, Yan Y, Jin X, et al. (2021) Microstructure and mechanical and thermal shock properties of hierarchically porous ceramics. *Ceram Int* 47: 24887–24894. https://doi.org/10.1016/j.ceramint.2021.05.215
11. Han L, Deng X, Li F, et al. (2018) Preparation of high strength porous mullite ceramics via combined foam-gelcasting and microwave heating. *Ceram Int* 44: 14728–14733. https://doi.org/10.1016/j.ceramint.2018.05.101
12. Ma B, Su C, Ren X, et al. (2019) Preparation and properties of porous mullite ceramics with high-closed porosity and high strength from fly ash via reaction synthesis process. *J Alloys Compd* 803: 981–991. https://doi.org/10.1016/j.jallcom.2019.06.272
13. Wang H, Li S, Li Y, et al. (2021) Preparation of novel reticulated prickly porous ceramics with mullite whiskers. *J Eur Ceram Soc* 41: 864–870. https://doi.org/10.1016/j.jeurceramsoc.2020.08.001
14. Li X, Li S, Yin Z, et al. (2023) Foam-gelcasting preparation and properties of high-strength mullite porous ceramics. *Ceram Int* 49: 6873–6879. https://doi.org/10.1016/j.ceramint.2022.10.096
15. Yang J, Zhang X, Zhang B, et al. (2022) Mullite ceramic foams with tunable pores from dual-phase sol nanoparticle-stabilized foams. *J Eur Ceram Soc* 42: 1703–1711. https://doi.org/10.1016/j.jeurceramsoc.2021.12.008
16. Hossain SS, Baek IW, Son HJ, et al. (2022) 3D printing of porous low-temperature in-situ mullite ceramic using waste rice husk ash-derived silica. *J Eur Ceram Soc* 42: 2408–2419. https://doi.org/10.1016/j.jeurceramsoc.2022.01.001
17. Huo X, Xia B, Hu T, et al. (2023) Effect of MoO_3 addition on fly ash based porous and high-strength mullite ceramics: In situ whisker growth and self-enhancement mechanism. *Ceram Int* 49: 21069–21077. https://doi.org/10.1016/j.ceramint.2023.03.242
18. Ma B, Su C, Ren X, et al. (2019) Preparation and properties of porous mullite ceramics with high-closed porosity and high strength from fly ash via reaction synthesis process. *J Alloys Compd* 803: 981–991.https://doi.org/10.1016/j.jallcom.2019.06.272

19. Kurovics E, Ibrahim JFM, Tihtih M, et al. (2020) Examination of mullite ceramic specimens made by conventional casting method from kaolin and sawdust. *J Phys Conf Ser* 1527: 012034. https://doi.org/10.1088/1742-6596/1527/1/012034
20. Martínez-Martínez S, Pérez-Villarejo L, Garzón E, et al. (2023) Influence of firing temperature on the ceramic properties of illite-chlorite-calcitic clays. *Ceram Int* 49: 24541–24557. https://doi.org/10.1016/j.ceramint.2022.11.077
21. Harrati A, Manni A, Hassani FO, et al. (2022) Potentiality of new dark clay-rich materials for porous ceramic applications in Ouled Sidi Ali Ben Youssef Area (Coastal Meseta, Morocco). *Bol Soc Esp Ceram Vidrio* 61: 130–145. https://doi.org/10.1016/j.bsecv.2020.08.003
22. Semiz B (2017) Characteristics of clay-rich raw materials for ceramic applications in Denizli region (Western Anatolia). *Appl Clay Sci* 137: 83–93. https://doi.org/10.1016/j.clay.2016.12.014
23. Yuan L, Ma B, Zhu Q, et al. (2017) Preparation and properties of mullite-bonded porous fibrous mullite ceramics by an epoxy resin gel-casting process. *Ceram Int* 43: 5478–5483. https://doi.org/10.1016/j.ceramint.2017.01.062
24. Kiran GS, Mukthapuram J, Yadav AK, et al. (2020) Effect of MoO_3 additive on fabrication of mullite based porous ceramics. *AIP Conf Proc* 2244: 040007. https://doi.org/10.1063/5.0009333
25. Zainudin FH, Zulkifli MS, Saud AS, et al. (2023) Formulation of Malaysian clay into inert ceramic balls: Effect of sintering temperature. *Mater Today Proc* 75: 197–201. https://doi.org/10.1016/j.matpr.2022.12.243
26. Zanelli C, Dondi M, Raimondo M, et al. (2010) Phase composition of alumina–mullite–zirconia refractory materials. *J Eur Ceram Soc* 30: 29–35. https://doi.org/10.1016/j.jeurceramsoc.2009.07.016
27. Wang W, Sun K, Liu H (2020) Effects of different aluminum sources on morphologies and properties of ceramic floor tiles from red mud. *Constr Build Mater* 241: 118119. https://doi.org/10.1016/j.conbuildmat.2020.118119
28. Hajian A, Artemenko A, Kromka A, et al. (2022) Impact of sintering temperature on phase composition, microstructure, and porosification behavior of LTCC substrates. *J Eur Ceram Soc* 42: 5789–5800. https://doi.org/10.1016/j.jeurceramsoc.2022.05.049
29. Wu D, Zhang H, Li L, et al. (2021) Effect of sintering temperature on structure and electrical transport properties of $La_{0.7}Ca_{0.26}Na_{0.04}MnO_3$ ceramics. *Ceram Int* 47: 12716–12724. https://doi.org/10.1016/j.ceramint.2021.01.131
30. Choudhary B, Anwar S, Medvedev DA, et al. (2022) Effect of sintering temperature on the transport properties of $La_2Ce_2O_7$ ceramic materials. *Ceram Int* 48: 6758–6766. https://doi.org/10.1016/j.ceramint.2021.11.227
31. Manullang RJ, Purnawan M, Taufik D, et al. (2022) The effect of pore former addition and sintering temperature on the characteristic of ceramic membrane. *AIP Conf Proc* 2391: 070017. https://doi.org/10.1063/5.0075598

AIMS Press